Ab initio calculations of the phonon spectra and the thermal expansion coefficients of the 4*d* metals

P. Souvatzis and O. Eriksson
Department of Physics, Uppsala University, Box 530, SE-75121 Uppsala, Sweden
(Received 9 July 2007; revised manuscript received 8 October 2007; published 24 January 2008)

We have performed first principles calculations of the phonon spectra of the 4*d* transition metals with the so-called supercell method and found good agreement with observations. Furthermore, the electron and phonon contributions to the free energy for the 4*d* metals have been calculated from a first principles method. From the free energy, the thermal expansion of the metals is calculated. The calculated thermal expansion coefficients for the cubic elements are in overall good agreement with the experiment when the local density approximation is employed, while the generalized gradient approximation calculations yield a discrepancy as big as ~30%. For the hexagonal elements, reasonable agreement is found between calculations and experiment for the volume thermal expansion at temperatures 200 K$\lesssim T\lesssim$300 K.

DOI: 10.1103/PhysRevB.77.024110 PACS number(s): 62.50.−p

I. INTRODUCTION

For the past two decades, *ab initio* methods have been used to calculate mechanical and thermodynamical properties of elements and compounds. However, in the beginning of the era of density functional theory, most of the calculations were done at $T=0$ K, or if done at finite temperature, the majority of the calculations were within the Debye-Grüneisen theory. One of the more extensive works on thermodynamical properties of nonmagnetic metals has been done by Moruzzi *et al.*[1] In this theoretical work, thermodynamical and mechanical properties of 14 nonmagnetic cubic metals were calculated within the context of the Debye-Grüneisen theory, where the average sound velocity used for calculating the Debye spectra was connected to the bulk modulus through an empirical value of Poisson's ratio. A similar approach was used for the actinides by Söderlind *et al.*[2]

In the present paper, we have continued the work by Moruzzi *et al.* by including the hexagonal nonmagnetic 4*d* elements. More importantly, we have taken a step beyond the Debye-Grüneisen theory by calculating the full phonon spectra in a quasiharmonic theory. The big advantage of this approach is that the calculations are entirely free of empirical parameters. In addition to this, we also provide here a set of first principles calculations of the phonon spectra of the 4*d* series and make a detailed comparison to experimental data.

II. CALCULATION OF THE FREE ENERGY

The Helmholtz free energy at a given strain $\bar{\epsilon}$ can be written as

$$F(\bar{\epsilon},T)=U(\bar{\epsilon})+F^{phon}(\bar{\epsilon},T)+F^{el}(\bar{\epsilon},T), \tag{1}$$

where $U(\bar{\epsilon})$ is the static lattice energy, F^{phon} the phonon free energy, and F^{el} the electron excitation free energy. The static lattice energy can be expressed as

$$U(\bar{\epsilon})=U_0+V\sum_{ij}C_{ij}\epsilon_i\epsilon_j+U^{anh}(\bar{\epsilon}), \tag{2}$$

where U_0 is the static lattice energy at zero strain, C_{ij} are the elastic constants, V is the equilibrium volume at $T=0$ K, and U^{anh} is the anharmonic contribution to the static lattice energy. For the cubic 4*d* metals, the static lattice energies have been calculated with the full potential linear muffin tin orbital (FP-LMTO) method[3] both within the local density approximation (LDA) and the generalized gradient approximation (GGA). In the FP-LMTO calculations, the number of k points in the irreducible part of the Brillouin zone was 752. To each eigenvalue, a Gaussian smearing of 20 mRy was applied to speed up the convergence of the calculation.[4]

For the hexagonal 4*d* metals, the anharmonic part of the static lattice energy was completely neglected, i.e., $U^{anh}(\bar{\epsilon})=0$, and only the elastic constants were used in the parametrization of the static lattice energy. To calculate the elastic constants of the hexagonal metals, the VASP code[5] was used, with a $30\times30\times20$ Monkhorst-Pack k-point mesh. Gaussian smearing of 0.2 eV of the electronic states and GGA projector augmented wave (PAW) potentials were used in all elastic calculations.

To evaluate the free energy contribution F^{phon}, which can be expressed as[6,7]

$$F^{phon}(\bar{\epsilon},T)=\int_0^\infty d\omega g(\omega,\bar{\epsilon})\left[\frac{\hbar\omega}{2}+k_BT\ln(1-e^{-\hbar\omega/k_BT})\right], \tag{3}$$

the phonon density of states $g(\omega,\bar{\epsilon})$ has to be calculated. This was done within the quasiharmonic approximation by making small displacements of the atoms in a supercell.[8]

For the phonon calculations, the VASP code was used, with a Monkhorst-Pack k-point mesh of $6\times6\times6$ for the fcc and bcc metals and $9\times9\times6$ for the hcp elements. Both LDA and GGA PAW potentials were used in the phonon calculations for the cubic metals, whereas for the hcp structures, only GGA PAW potentials were used. Gaussian smearing of 0.2 eV was used in all the phonon calculations. The phonon density of states was then calculated with the code in Ref. 9 where an $80\times80\times80$ k-point mesh was used with a 0.05 THz smearing.

The free electronic energy was calculated by the approximate expression given by Sommerfeld and Frank,[10]

$$F^{el}(\bar{\epsilon},T) = -\frac{(\pi k_B)^2}{6} D(\epsilon_F,\bar{\epsilon}) T^2, \quad (4)$$

where $D(\epsilon_F,\bar{\epsilon})$ is the electronic density of states at the Fermi level. Finally, it should be stressed that even though the phonon dispersions presented in this work have been calculated at the experimental lattice constants, only theoretically calculated lattice constants have been used in all the thermodynamic calculations.

III. THERMAL EXPANSION AND THE PHONON SPECTRA OF THE CUBIC METALS

For the cubic metals, the free energy [Eq. (1)] depends only on the temperature and the volume strain $\epsilon_v \equiv d[\ln(V)]$, i.e., $F(\bar{\epsilon},T)=F(\epsilon_v,T)$. Here, the phonon density of states was calculated for seven different volume strains in steps of 0.0025 Å. Due to the symmetry of the cubic metals, only one displacement was needed to obtain the full force constant matrix. The displaced atom was in the (0, 0, 0) position of the supercell and the directions of the displacements were $[1\bar{1}0]$ and [001] for the fcc and bcc elements, respectively, with amplitudes equal to ~0.3% of the lattice constant. The supercells used for calculating the phonon contribution to the free energy were $3\times3\times3$ cells (27 atoms) for Pd and Ag and $4\times4\times4$ (64 atoms) cells for Rh, Nb, and Mo. In order to check the convergence of the phonon calculations of the 4*d* bcc metals, additional $6\times6\times6$ (216 atoms) supercell calculations were performed within the GGA. For convergence tests on the fcc 4*d* metals, we refer to the work by Grabowski *et al.*[11]

In Figs. 1 and 2, we show the calculated phonon dispersions for the 4*d* cubic metals together with experimental data. Here, excellent agreement is found between the calculated and experimental phonon frequencies for almost all cubic 4*d* elements. The only exception is Mo, where the calculated frequencies around the *H* and *N* symmetry points are somewhat smaller than the experimental frequencies. Keeping the effective number of *k* points constant in the Mo calculations, no significant improvement can be seen as the cell size is increased from 64 atoms (black dotted curve in the lower panel of Fig. 2) to 216 atoms (solid red curve in the lower panel of Fig. 2). However, when the *k*-point mesh is increased from $4\times4\times4$ to $5\times5\times5$ in the 216-atom GGA calculation, the calculated Mo phonons are in overall acceptable agreement with observed data (solid blue curve in the lower panel of Fig. 2).

In the 64 atom calculations of Nb, imaginary frequencies were obtained in the long wavelength limit. This unphysical mechanical instability corresponds to negative values of the C_{44} elastic constant. Observe that in the results of the Nb 64-atom calculations (black dotted curve and solid black curve in the upper panel of Fig. 2), the imaginary frequencies corresponding to negative values of C_{44} have been replaced by phonon frequencies calculated from separately calculated elastic constants. We will describe the details of this calculation below.

In an attempt to remedy the error observed for the long wavelength phonons of Nb, the cell size in the Nb calculations was increased to 216 atoms (solid red and blue curve in the upper panel of Fig. 2). Here, the imaginary frequencies are observed to have completely disappeared, even though the discrepancy between theory and experiment is still noticeable, with a softening of the transverse mode along the Γ to *H* symmetry direction and one between the *H* and *P* symmetry points. Increasing the *k*-point mesh from $4\times4\times4$ (solid red curve in the upper panel of Fig. 2) to $5\times5\times5$ (solid blue curve in the upper panel of Fig. 2) does not significantly change the outcome of the calculation, suggesting that the calculation is converged with respect to the number of *k* points and that the discrepancy found between the presently calculated Nb phonons and experimental data stems from finite size effects.

Due to the computational cost involved in performing repeated phonon calculations with the larger 216-atom cell, the 64-atom cells had to be used in the thermal expansion calculations of Nb and Mo. Thus, a more difficult approach had to be used in the phonon calculations of Nb, where the negative C_{44}'s were replaced by separately calculated C_{44} constants. The imaginary long wave phonons were then replaced with phonon frequencies obtained from the calculated set of elastic constants. The C_{44} were calculated with the PAW potentials within the GGA. At the experimental room temperature

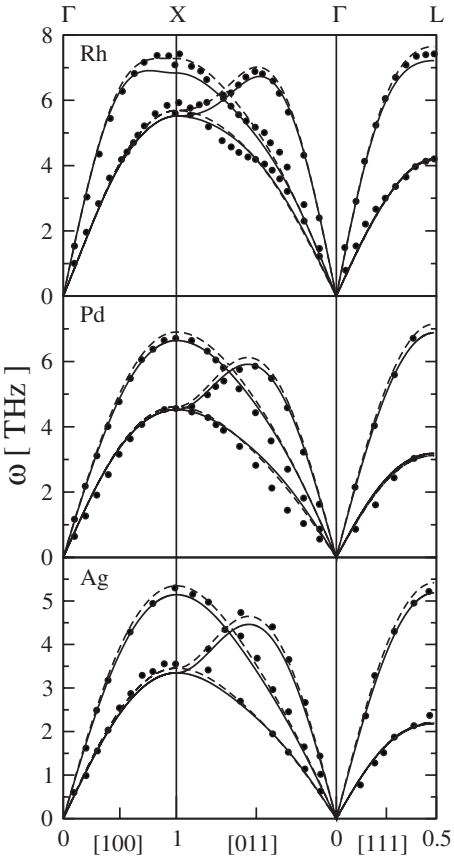

FIG. 1. The phonon dispersion of the fcc 4*d* metals at ambient pressure. The solid curves are the present $T=0$ K LDA calculation at the experimental volumes. The dashed curves are the present $T=0$ K GGA calculation at the experimental volumes. The filled circles are the experimental room temperature data of Refs. 19–21.

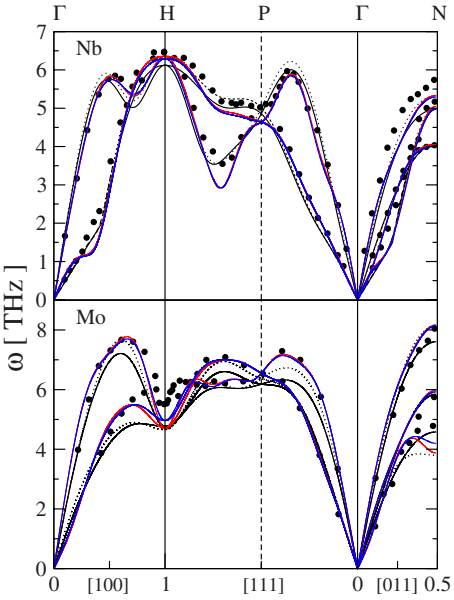

FIG. 2. (Color online) The phonon dispersion of the bcc 4*d* metals at ambient pressure. The solid black curves are the present $T=0$ K LDA calculation done with a 64-atom supercell with a $6\times6\times6$ k-point mesh, the dotted black curves are the present $T=0$ K GGA calculation done with a 64-atom supercell with a $6\times6\times6$ k-point mesh, and the solid red and blue curves are the present $T=0$ K GGA calculation done with a 216-atom supercell with a $4\times4\times4$ and a $5\times5\times5$ k-point mesh, respectively. All calculations have been done at the experimental room temperature equilibrium volumes. The filled circles are the experimental room temperature data of Refs. 22 and 23.

volume, the calculations gave $C_{44}=21$ GPa, which can be compared with the experimental room temperature value of 31 GPa or to the value calculated by Söderlind *et al.*[12] of 27 GPa.

By fitting the calculated free energy to the Vinet EOS[13] at different temperatures and minimizing the free energy with respect to volume at each temperature, the thermal expansion of the cubic metals was obtained. In Figs. 3 and 4, we show the calculated thermal expansions for the 4*d* cubic metals together with experimental data. Here, good agreement is found between theory and experiment for all the fcc and bcc elements of the 4*d* series when the LDA is used. However, when the GGA was used, the thermal expansion coefficients are overestimated, sometimes by as much as ~30%.

The discrepancy between the LDA and GGA calculations can, in the case of the 4*d* cubic metals, be attributed to the overestimation of the product between the zero temperature isothermal bulk modulus and zero temperature equilibrium volume BV_0, calculated within the LDA, which is most easily seen from the fact that the thermal expansion to a good approximation can be expressed as

$$\alpha(T) = -\frac{1}{3BV_0}\frac{\partial^2 F^{phon}(\epsilon_v, T)}{\partial T \partial \epsilon_v}. \quad (5)$$

In Table I, the calculated bulk moduli and pressure derivatives of the bulk moduli for the cubic 4*d* metals are shown

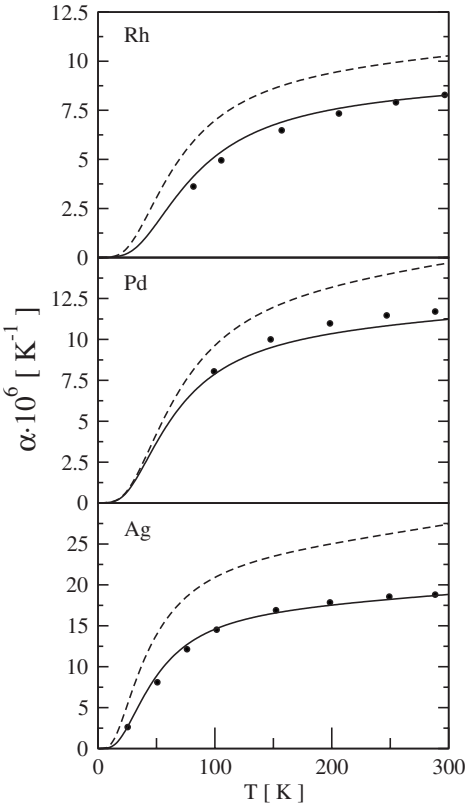

FIG. 3. Linear thermal expansion for the fcc 4*d* metals at ambient pressure. The solid lines are the theoretical thermal expansions calculated within the LDA. The dashed lines are theoretical thermal expansions calculated within the GGA. The filled circles are the experimental data of Ref. 24.

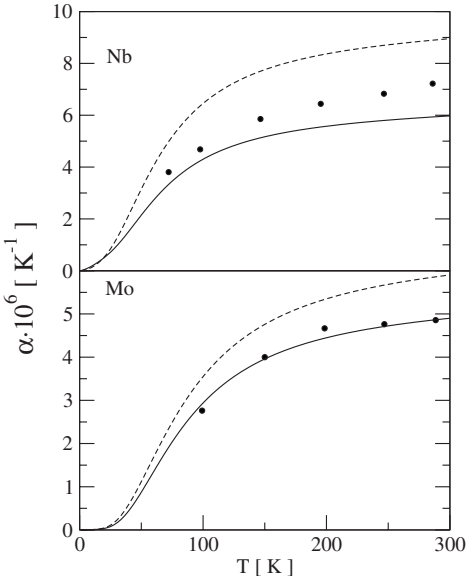

FIG. 4. Linear thermal expansion for the bcc 4*d* metals at ambient pressure. The solid lines are the theoretical thermal expansions calculated within the LDA. The dashed lines are theoretical thermal expansions calculated within the GGA. The filled circles are the experimental data of Ref. 24.

TABLE I. The calculated bulk moduli B (GPa) and pressure derivatives of the bulk moduli $B'=\partial B/\partial P$ of the 4d cubic metals, here presented together with experimental data. The experimental data for the bulk moduli have been measured at $T=4.2$ K and are taken from Refs. 14 and 15. The experimental data for B' are taken from Refs. 16 and 18. The theoretical values of B and B' have all been calculated at the theoretical $T=0$ K equilibrium volumes.

	$B^{(LDA)}$	$B'^{(LDA)}$	$B^{(GGA)}$	$B'^{(GGA)}$	$B^{(expt)}$	$B'^{(expt)}$
Nb	192	3.77	173	2.58	173	4.1
Mo	291	4.21	262	3.96	265	4.70
Rh	318	5.03	250	4.98	267	4.50
Pd	227	5.41	169	5.18	195	5.42
Ag	138	5.65	91	5.22	109	5.87

together with experimental data, and in Tables II and III, the calculated and experimental lattice constants are displayed for all the 4d metals.

Despite the overestimation of BV_0, the thermal expansion coefficients calculated within the LDA show good agreement with experimental data, with the exception of Nb. The reason for this is that the error from the overestimated product BV_0 is canceled by the overestimation of the second derivative $\partial^2 F^{phon}/\partial T \partial \epsilon_v$ which is readily verified by inspection of Eq. (5). We also note that in the work of Grabowski *et al.*,[11] the thermal expansion of several 4d and 5d fcc metals were also found to be overestimated by the GGA.

IV. THERMAL EXPANSION AND THE PHONON SPECTRA OF THE hcp METALS

To parametrize the phonon part of the free energy, the phonon density of states was calculated for seven different volume strains

$$(\epsilon_v, \epsilon_c) = (0,0), (\pm 0.006, 0), (\pm 0.012, 0), (\pm 0.018, 0)$$

and six different strains along the c axis

$$(\epsilon_v, \epsilon_c) = (0, \pm 0.002), (0, \pm 0.004), (0, \pm 0.006)$$

relative to the calculated $T=0$ K equilibrium lattice constants and c/a ratios. Here, the volume and tetragonal strains are defined by $\epsilon_v \equiv d[\ln(V)]$ and $\epsilon_c \equiv d[\ln(c/a)]$.

To obtain the full force constant matrix for the hcp lattice, the atom in the (0, 0, 0) position of the supercell was displaced in two directions. The directions of the displacements were [110] and [001] with amplitudes that were equal to ~0.4% of the lattice constant. The supercell used was a $3\times3\times2$ cell.

In Fig. 5, we show the calculated phonon dispersions for the 4d hcp metals together with experimental data. Here, it is seen that the calculated phonon frequencies show good agreement with experimental data, in general, and the agreement is best for the acoustic phonons in the long wavelength limit. The biggest discrepancy between theory and experiment can be found along the Γ to A symmetry line for the $3\times3\times2$ supercell calculation of Tc (dashed curve in the second panel from the bottom in Fig. 5). Here, an entire optical mode is missing due to a twofold degeneracy introduced by the limited size of the supercell. This is corrected in the $4\times4\times3$ supercell calculation of Tc (solid curve in the second panel from the bottom in Fig. 5) in which the missing branch is present. Also in the case of Ru, using the larger $4\times4\times3$ cell (solid curve in the bottom panel of Fig. 5) greatly improves the agreement between theory and experiment. Calculations were also done with the larger $4\times4\times3$ cell for both Y and Zr (results not shown), but no improvement of the agreement between theory and experiment was obtained. However, due to the computational cost involved in performing repeated phonon calculations with the bigger $4\times4\times3$ supercell, the thermal expansion calculations of the hexagonal 4d metals were done with the smaller $3\times3\times2$ supercell.

By differentiating the free energy [Eq. (1)] with respect to ϵ_v and ϵ_c at equilibrium strain, it is possible to obtain an expression for the change in volume and structural property as a function of temperature. These changes are expressed in terms of equilibrium strains, ϵ_v^0 and ϵ_c^0, and can be written in terms of elastic constants and strain derivatives of the free energy,

TABLE II. The calculated zero temperature lattice constants a (Å) of the 4d cubic metals, here presented together with experimental data. The experimental data are taken from Ref. 17.

	$a^{(LDA)}$	$a^{(GGA)}$	$a^{(expt)}$
Nb	3.26	3.31	3.30
Mo	3.12	3.17	3.15
Rh	3.76	3.85	3.80
Pd	3.85	3.96	3.89
Ag	4.00	4.16	4.09

TABLE III. The calculated zero temperature lattice constants a and c (Å) of the 4d hcp metals, here presented together with experimental data. The experimental data are taken from Ref. 17.

	$a^{(GGA)}$	$c^{(GGA)}$	$a^{(\mathrm{expt})}$	$c^{(\mathrm{expt})}$
Y	3.65	5.65	3.65	5.73
Zr	3.24	5.17	3.23	5.15
Tc	2.76	4.42	2.74	4.39
Ru	2.74	4.32	2.71	4.28

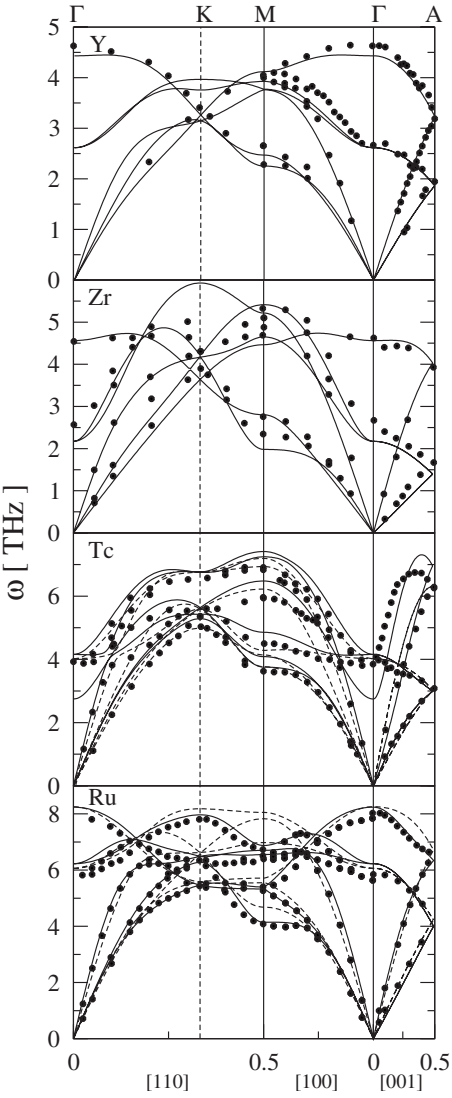

FIG. 5. The phonon dispersion of the hcp 4*d* metals at ambient pressure. The solid curves are the present $T=0$ K calculation at the experimental volumes. In the case of Tc and Ru, the solid curve is the present calculation done with a $4\times4\times3$ supercell and the dashed curve is the present calculation done with a $3\times3\times2$ supercell. The filled circles are the experimental room temperature data of Refs. 27–30.

$$\epsilon_v^0(T) = \frac{1}{V(B_{11}B_{22} - B_{12}^2)}\left[- B_{22}\frac{\partial F^*}{\partial \epsilon_v} + B_{12}\frac{\partial F^*}{\partial \epsilon_c}\right], \quad (6)$$

$$\epsilon_c^0(T) = \frac{1}{V(B_{11}B_{22} - B_{12}^2)}\left[B_{12}\frac{\partial F^*}{\partial \epsilon_v} - B_{11}\frac{\partial F^*}{\partial \epsilon_c}\right], \quad (7)$$

where

$$B_{11} = \frac{2}{9}\left(C_{11} + C_{12} + \frac{1}{2}C_{33} + 2C_{13}\right), \quad (8)$$

$$B_{22} = \frac{2}{9}(C_{11} + C_{12} + 2C_{33} - 4C_{13}), \quad (9)$$

$$B_{12} = \frac{1}{9}(C_{33} + C_{13} - C_{11} - C_{12}), \quad (10)$$

$$F^* = F^{ph} + F^{el}. \quad (11)$$

Furthermore, by differentiating Eqs. (6) and (7) with respect to the temperature, the following relations are obtained for the thermal expansion coefficients:[31]

$$\alpha_\perp = \frac{1}{3V(B_{11}B_{22} - B_{12}^2)}\left[- (B_{22} + B_{12})\frac{\partial^2 F^*}{\partial T \partial \epsilon_v} + (B_{12} + B_{11})\frac{\partial^2 F^*}{\partial T \partial \epsilon_c}\right], \quad (12)$$

$$\alpha_\parallel = \frac{1}{3V(B_{11}B_{22} - B_{12}^2)}\left[- (B_{22} - 2B_{12})\frac{\partial^2 F^*}{\partial T \partial \epsilon_v} + (B_{12} - 2B_{11})\frac{\partial^2 F^*}{\partial T \partial \epsilon_c}\right], \quad (13)$$

$$\beta = \frac{1}{V(B_{11}B_{22} - B_{12}^2)}\left[- B_{22}\frac{\partial^2 F^*}{\partial T \partial \epsilon_v} + B_{12}\frac{\partial^2 F^*}{\partial T \partial \epsilon_c}\right], \quad (14)$$

where $\alpha_\perp = \frac{1}{a}\frac{da}{dT}$, $\alpha_\parallel = \frac{1}{c}\frac{dc}{dT}$, and $\beta = \frac{1}{V}\frac{dV}{dT}$.

By fitting the free energies $F[\epsilon_v, \epsilon_c] = F[\epsilon_v, 0]$ and $F[\epsilon_v, \epsilon_c] = F[0, \epsilon_c]$ at a given temperature to polynomials of first degree in ϵ_v and in ϵ_c, the equilibrium strains can be obtained from Eqs. (6) and (7), and the thermal expansion coefficients can be calculated from Eqs. (12)–(14), using calculated values of the elastic constants. In Table IV, the calculated elastic constants of the hexagonal 4*d* metals (excluding C_{55}) are shown together with their respective experimental values. We note in passing that experimental and theoretical values of the elastic constants are in good agreement and that the present calculation yields values similar values to that by Fast *et al.*[25]

In Fig. 6, we show the calculated thermal expansion coefficients of the hcp 4*d* metals. Here, the best agreement between theory and experiment is found for the volume thermal expansion coefficients β in the temperature interval $200\ \text{K} \lesssim T \lesssim 300\ \text{K}$. Also, the theoretical thermal expansion coefficients $\alpha_\perp$ for Zr and Ru are in fairly good agreement with the experimental data for temperatures $\gtrsim 100$ K. The biggest discrepancy between theory and experiment appears for the thermal expansion coefficient $\alpha_\parallel$ in Zr. Not only is the theoretical prediction of $\alpha_\parallel$ considerably smaller than the corresponding experimental data but also negative for $T \lesssim 75$ K. However, the experimental data for Zr display some peculiar features, especially the thermal expansion coefficients $\alpha_\perp$ and β, which show only the slightest variation across the entire temperature interval. Furthermore, if one would extrapolate the experimental $\alpha_\perp$ and β along their respective tangents at $T \sim 50$ K down to 0 K, they would be positive and considerably different from zero. A general property of all materials is that the thermal expansion coefficients should approach zero at $T=0$ K. This is the situation for hcp Ti which is isoelectronic to Zr. It is a matter of fact that hcp Ti has a general behavior of $\alpha_\perp$ and $\alpha_\parallel$ correspond-

TABLE IV. The theoretical and experimental elastic constants of the 4*d* hexagonal metals.

	C_{11}	C_{12}	C_{13}	C_{33}	C_{55}
Y [GPa]	83.0	21.0	21.0	83.1	
Y[a] [GPa]	83.4	29.1	19.0	80.1	26.9
Zr [GPa]	150.5	53.4	71.0	169.0	
Zr[a] [GPa]	155.4	67.2	64.6	172.5	36.3
Tc [GPa]	584.3	207.5	186.5	541.2	
Tc[b] [GPa]	433.0	199.0	199.0	470.0	177.0
Ru [GPa]	562.4	178.8	158.2	605.1	
Ru[a] [GPa]	576.3	187.2	167.3	640.5	189.1

[a]Experimental data measured at 4.2 K taken from Ref. 14.
[b]Experimental data from Ref. 26. Here, the elastic constant C_{55} has not been calculated since it is not used in the parametrization of the static lattice energy of the 4*d* hcp metals. The theoretical values of elastic constants have all been calculated at the theoretical $T=0$ K equilibrium volumes.

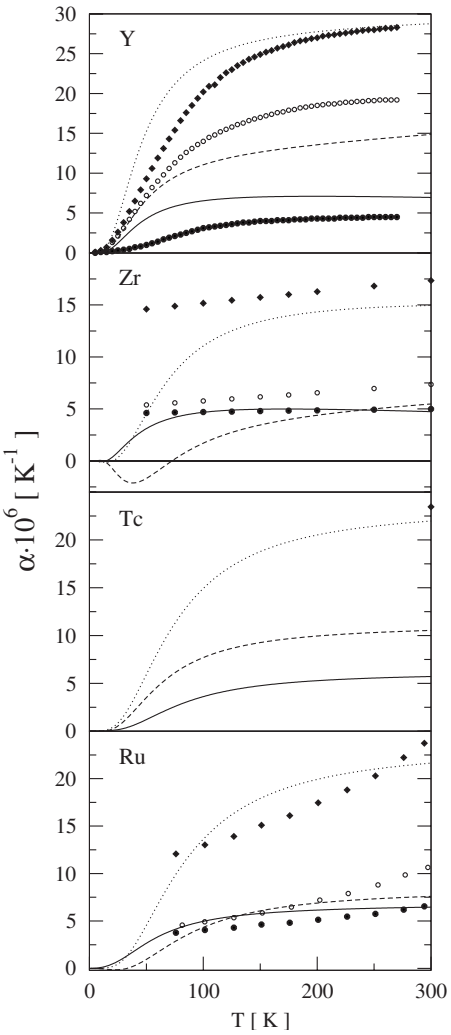

FIG. 6. Linear thermal expansion for the hcp 4*d* metals at ambient pressure. The solid lines, the dashed lines, and the dotted lines are the thermal expansion coefficients $\alpha_{\perp}$, $\alpha_{\parallel}$, and β, respectively, of the present calculation. The filled circles, the empty circles, and the filled diamonds are the experimental thermal expansion coefficients, $\alpha_{\perp}$, $\alpha_{\parallel}$, and β, respectively, of Refs. 32–34. The experimental data for Tc have been calculated from the polycrystalline thermal expansion coefficient $\alpha=\beta/3$.

ing to the curves for Zr in Fig. 6.[35] The lack of such behavior in the experimental data of Zr (and indeed the data for Ru also seem to suggest such a behavior, although data were only taken down to ~75 K) suggests that the experimental thermal expansion data of Zr are indeed somewhat questionable. However, due to the long range nature of the Zr force constants,[36] which is considerable compared to the isoelectronic elements Ti and Hf, and due to the observed substantial temperature dependence of the phonons in hcp Zr,[37,38] finite size effects and temperature effects, such as the smearing of the Fermi surface (FS) and the anharmonicity beyond the effect of thermal expansion, should also be taken into consideration when one tries to understand the origin of the discrepancy between the theoretical and experimental thermal expansions of hcp Zr and might be important for an accurate evaluation of the free energy as a function of temperature for hcp Zr. We have, however, not pursued this approach since we wanted to treat all 4*d* elements on equal footing.

Despite the shortcomings in the thermal expansion calculations of the 4*d* bcc and hcp elements, the present theoretical study reproduces the room temperature polycrystalline thermal expansion trend all across the 4*d* transition metal series. This is obvious from Fig. 7 where we show the volume thermal expansion for the entire 4*d* series at room temperature ($T=300$ K) and ambient pressure together with experimental data.

V. CONCLUSION

From *ab initio* calculations, the phonon spectra and the thermal expansion coefficients for the 4*d* elements have been calculated. For the cubic structures, the present LDA calculations show good agreement with experimental data, both concerning phonon spectra and thermal expansions. For the GGA calculations, the agreement between theory and experiment is only good in the case of the phonon spectra, while for the thermal expansions, the discrepancy is sometimes as high as ~30%. In both the LDA and the GGA calculations of the 4*d* cubic metals, the second derivative $\partial^2 F^{phon}/\partial T \partial \epsilon_v$ of the phonon contribution to the free energy was found

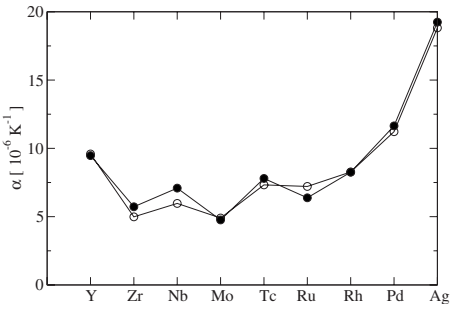

FIG. 7. Linear thermal expansion for the 4*d* metals at room temperature and ambient pressure. The empty circles are the present calculation. Here, the theoretical data for the cubic elements are taken from the LDA calculations. The filled circles are the experimental data of Ref. 34. For the hexagonal elements, the polycrystalline expansion coefficients $\alpha \equiv \beta/3$ are displayed.

to be overestimated. However, this overestimation was almost completely canceled by the overestimation of BV_0 in the LDA calculations, whereas no such cancellation was found in the GGA calculations. In the case of the hcp 4*d* elements, the calculated phonon spectra and thermal volume expansion agree with experiment. Concerning the linear thermal expansion along the *c* and *a* axes, the agreement is less good, especially for Y and Zr. However, not only the increase of supercell size might suffice to improve on the calculated results for the hcp 4*d* elements. The inclusion of the anharmonic contribution to the static lattice energy and a more elaborate parametrization of the phonon contribution to the free energy could also improve the agreement between theory and experiment, especially at high temperatures.

ACKNOWLEDGMENTS

We are grateful to the Strategic Foundation for Research (SSF), the Swedish Research Council (VR), the Swedish National Supercomputer Center (NSC), UPMAX, and to the Göran Gustafsson foundation, for support. Valuable discussions with M. Katsnelson are acknowledged.

[1] V. L. Moruzzi, J. F. Janak, and K. Schwarz, Phys. Rev. B **37**, 790 (1988).
[2] P. Söderlind, L. Nordström, Youngming Lou, and B. Johansson, Phys. Rev. B **42**, 4544 (1990).
[3] J. M. Wills and B. R. Cooper, Phys. Rev. B **36**, 3809 (1987); D. L. Price and B. R. Cooper, *ibid.* **39**, 4945 (1989); J. M. Wills, O. Eriksson, and M. Alouani, in *Electronic Structure and Physical Properties of Solids*, edited by H. Dreysse (Springer, Berlin, 2000), p. 148.
[4] M. Methfessel and A. T. Paxton, Phys. Rev. B **40**, 3616 (1989).
[5] G. Kresse and J. Furthmuller, Phys. Rev. B **54**, 11169 (1996).
[6] D. C. Wallace, *Thermodynamics of Crystals* (Wiley, New York, 1972).
[7] G. K. Straub, J. B. Aidun, and J. M. Wills, C. R. SanchezCastro, and D. C. Wallace, Phys. Rev. B **50**, 5055 (1994).
[8] P. Souvatzis, A. Delin, and O. Eriksson, Phys. Rev. B **73**, 054110 (2006).
[9] D. Alfé, The PHON software can, together with a description of the program, be found at http://chianti.geol.ucl.ac.uk/dario/
[10] A. Sommerfeld and N. H. Frank, Rev. Mod. Phys. **3**, 1 (1931).
[11] B. Grabowski, T. Hickel, and J. Neugebauer, Phys. Rev. B **76**, 024309 (2007).
[12] P. Söderlind, O. Eriksson, J. M. Wills, and A. M. Boring, Phys. Rev. B **48**, 5844 (1993).
[13] P. Vinet, J. R. Smith, J. Ferrante, and J. H. Rose, Phys. Rev. B **35**, 1945 (1987).
[14] G. Simmons and H. Wang, *Single Crystal Elastic Constants and Calculated Aggregate Properties: A Handbook* (MIT, Cambridge, 1971).
[15] E. Walker, J. Ashkenazi, and M. Dacorogna, Phys. Rev. B **24**, 2254 (1981).
[16] J. H. Rose, J. R. Smith, F. Guinea, and J. Ferrante, Phys. Rev. B **29**, 2963 (1984).
[17] A. Taylor and B. J. Kagle, *Crystallographic Data on Metal and Alloy Structures* (Dover, New York, 1963).
[18] S. Raju, E. Mohandas, and V. S. Raghunathan, J. Phys. Chem. Solids **58**, 1367 (1997).
[19] A. Eichler, K.-P. Bohnen, W. Reichardt, and J. Hafner, Phys. Rev. B **57**, 324 (1998).
[20] Barry L. Fielek, J. Phys. F: Met. Phys. **10**, 2381 (1980).
[21] G. Nilsson and S. Rolandson, Phys. Rev. B **7**, 2393 (1973).
[22] A. D. B. Woods and S. H. Chen, Solid State Commun. **2**, 233 (1964).
[23] Y. Nakagawa and A. D. B. Woods, Phys. Rev. **11**, 271 (1963).
[24] R. K. Kirby, T. A. Hahn, and B. D. Rothrock, *American Institute of Physics Handbook* (McGraw-Hill, New York, 1957), Sec. 4f.
[25] L. Fast, J. M. Wills, B. Johansson, and O. Eriksson, Phys. Rev. B **51**, 17431 (1995).
[26] *Second and Higher Order Elastic Constants*, Landolt-Börnstein, Group III (Springer, New York, 1992), pp. 118–128.
[27] S. K. Sinha, T. O. Brun, L. D. Muhlestrin, and J. Sakurai, Phys. Rev. B **1**, 2430 (1970).
[28] N. Wakabayashi, R. H. Scherm, and H. G. Smith, Phys. Rev. B **25**, 5122 (1982).
[29] R. Heid, L. Pintschovius, W. Reichardt, and K.-P. Bohnen, Phys. Rev. B **61**, 12059 (2000).
[30] C. Stassis, J. Zarestky, D. Arch, O. D. McMasters, and B. N. Harmon, Phys. Rev. B **18**, 2632 (1978).
[31] V. P. Antropov, M. I. Katsnelson, V. G. Koreshkov, A. I. Likhtenstein, A. V. Trefilov, and V. G. Vaks, Phys. Lett. A **130**, 155 (1988).
[32] R. W. Meyerhoff and F. Smith, J. Appl. Phys. **33**, 219 (1962).
[33] J. Goldak, L. T. Lloyd, and C. S. Barrett, Phys. Rev. **144**, 478 (1966).
[34] Y. S. Touloukian, R. K. Kirby, R. E. Taylor, and P. D. Desai, *Thermal Expansion, Metallic Elements and Alloys* (Plenum, New York, 1975).
[35] P. Souvatzis, O. Eriksson, and M. I. Katsnelson, Phys. Rev. Lett. **99**, 015901 (2007).
[36] I. Schnell, M. D. Jones, S. P. Rudin, and R. C. Albers, Phys. Rev. B **74**, 054104 (2006).
[37] E. S. Fisher and C. J. Renken, Phys. Rev. **135**, A482 (1964).
[38] C. Stassis, J. Zarestky, D. Arch, O. D. McMasters, and B. N. Harmon, Phys. Rev. B **18**, 2632 (1978).